F. Trevisi, M. McWilliam, M. Gaunaa
Configuration Optimization and Global Sensitivity Analysis of Ground-Gen and Fly-Gen Airborne Wind Energy Systems
Renewable Energy, Vol. 178, 2021, p. 385-402
doi:10.1016/j.renene.2021.06.011

Configuration optimization and global sensitivity analysis of *Ground-Gen* and *Fly-Gen* Airborne Wind Energy Systems

Filippo Trevisi[a,1,*], Michael McWilliam[a], Mac Gaunaa[a]

[a] *DTU Wind Energy, Frederiksborgvej 399, 4000 Roskilde, Denmark*

Abstract

This paper presents an analysis and optimization of Airborne Wind Energy Systems (*AWESs*), designed to maximize the Annual Energy Production (*AEP*) and, in the second part, the economic profit. A gradient-based optimization algorithm is used to perform the preliminary design of the main *AWES* sub-systems. A global sensitivity analysis is carried out to study how the design process, represented by the optimization problem, is influenced by aleatory and epistemic uncertainties. In particular, *Ground-Gen* and *Fly-Gen AWESs* are studied with a unified model to allow for a quantitative comparison. In the first part of the work, an ideal hybrid *AWES* design with ground and on-board power generation is considered. With this approach, the common characteristics of *Ground-Gen* and *Fly-Gen AWES* designs that maximize *AEP* are found. In the second part, *Ground-Gen* and *Fly-Gen AWES* optimal economic designs are analyzed individually. It is found that a fully developed *AWES* has strong potential to be highly competitive in the energy market, by providing cheap renewable energy. *Fly-Gen AWESs* are found to be slightly more profitable than *Ground-Gen* if the airborne unit is not replaced often. The main physical and economical characteristics of optimal designs are highlighted.

Keywords: AWES, Configuration optimization, Global sensitivity analysis, Uncertainty quantification, Sobol indices

*Corresponding author. E-mail address: filippo.trevisi@polimi.it (F. Trevisi).

[1] Permanent address: Politecnico di Milano, Department of Aerospace Science and Technology, Via La Masa, 34 20156 Milano, Italy

1. Introduction

Airborne Wind Energy (*AWE*) is the branch of Wind Energy which makes use of airborne devices to harvest power from the high altitude wind [1, 2]. Compared to conventional wind turbines, Airborne Wind Energy Systems (*AWESs*) can reach higher altitudes, thus better wind resources, and they are characterized by lighter systems, driving down the mass-related costs. Given the promising features of this technology, the *AWE* community, composed by small and medium-sized enterprises and research institutions, is gradually expanding [3]. Airborne Wind Energy Systems are classified based on the way the lift force, used for the power production, is generated. This work focuses on the *AWESs* which generate power by flying crosswind. The power equation of Crosswind *AWESs* was first theorized by Loyd [4] in 1980. He showed that Crosswind *AWESs* can generate power in two ways. The first type makes use of an electric generator placed on the ground: *Ground-Gen AWESs* produce power by pulling the tether and unwinding the generator. *Ground-Gen AWESs* can use soft kites [5, 6] or rigid wing kites [7, 8]. The second crosswind *AWES* type generates power with small on-board wind turbines: *Fly-Gen AWESs* produce power on-board and transmit it to the ground through the tether [9, 10]. Companies and research institutions are evenly exploring the two generation types, but no concept has proven superior yet. Qualitative thoughts or considerations on the final design performances are mostly driving the comparison between the two crosswind generation types [11]. The aim of this work is to perform a quantitative comparison [12], by assessing the two generation types with a unified model [13] and with the same methods. This work focuses on rigid wing kites. The unified model, presented in [13], is coupled with an optimization algorithm, which performs a system design to maximize the annual energy production (*AEP*) and, later, the profit of a company operating a *AWES*.

Studies of this type have been carried out for *Ground-Gen* and *Fly-Gen AWESs* individually. Concerning *Ground-Gen*, Heilmann et al. [14] economically evaluated an *AWES* wind farm composed of soft kites and performed a sensitivity analysis on the design. They found that the *LCOE* for their design is ranging between 40 and 110 €/MWh. Grete [15] in his Master thesis developed a framework for the optimization of *AWESs* based on soft kites, stating that the *LCOE*, with improvements of the airborne unit, are likely to range from 40 to 60 €/MWh. Concerning *Fly-Gen*, Bauer et al. [16] developed an optimization framework for an utility-scale system design. Their main hypothesis is that if the lift coefficient is maximized, the power, annual energy production, allowed costs and profit margin are also maximized. They therefore propose a design based on a biplane aircraft to increase the wing bending stiffness, such that the lift coefficient and the related loading can be set to extremely high values.

The present work aims to establish a methodology for the *AWES* system design and optimization and to give a quantitative comparison between the two technologies. While performing the comparison, a number of research question related to *AWESs* in the future are investigated. The final goal of this work is to identify trends in the design, strengths and weaknesses of design choices and crucial research topics needed to enable the technology.

This paper is organised as follows:

In Section 2 the methods used to evaluate the model proposed in [13] are introduced and explained. A gradient based optimization algorithm is used to perform the design of *AWESs*. Later, the influence of model parameters (*i.e.* parameters that are fixed within the optimization problem) on the optimization problem is studied with a global sensitivity analysis.

In Section 3, the global sensitivity analysis results of designs maximizing the annual energy production are presented. The model used in this section is the unified physical model proposed in [13]. This model can analyse ground and on-board power generation and combinations thereof for rigid wing kites. The aim of this investigation is to study the optimal *AWESs* from a pure power production point of view.

In Section 4, the global sensitivity analysis results of designs maximizing the profit are presented. A cost is associated to the designs according to the model described in [13] and the economic performances are evaluated. In this part, *Ground-Gen* and *Fly-Gen* are evaluated individually, to point out the differences, strengths and weaknesses of the two generation types.

The work presented in this paper is based on the models developed in [12], which have been refined in [13], and on the methods presented in [12], which are here used again. This work is therefore the continuation of [13].

2. Design evaluation methods

This research evaluates the model [13] through a 2-stage process summarized in Figure 1. The first evaluation stage is an optimization, the second is a global sensitivity analysis.

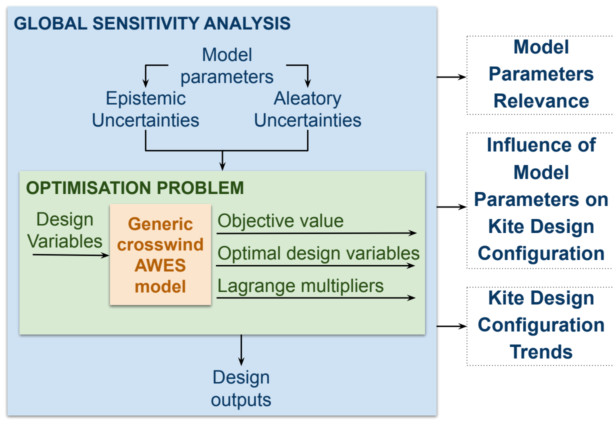

Figure 1: Evaluation framework of the unified *AWES* model.

Considering the first stage, the design process of an *AWES* is modelled as an optimization problem. The optimizer modifies the design variables, which are model inputs, to minimize the objective function, which is a model output. The result of the optimization is the objective value achieved by the design, the optimal design variables, and the Lagrange multipliers. Lagrange multipliers are properties of the optimal solution and indicate how much the objective function would improve with respect to changes in the given constraint limit. This is described in more detail in Section 2.1.
The optimization is based on a set of parameters that are held constant. These parameters can represent environmental factors (*e.g.* wind resource), technological capabilities (*e.g.* efficiency of the power generation) and economic parameters (*e.g.* material costs). Currently, the authors do not have accurate estimates for many of these parameters. Furthermore, an important challenge in analyzing design trends in *AWE* is that the technology is still in a state of development. Unlike conventional wind turbines, there is not a established configuration or a history of functioning commercial products. Thus, we have to consider how the design trends will evolve in the future. For this reason, many of these fixed parameters are treated as uncertain variables in the second stage of the analysis.
At the time of design in the future, these uncertain parameters would become known and incorporated into the design process, thus the effect of this uncertainty is on the design process itself. To understand the impact of this uncertainty, this research employs uncertainty quantification about the optimization.

It is therefore studied in the second evaluation stage (Figure 1) how the fully deterministic design process (*i.e.* the optimization problem) is influenced by the uncertain model parameters. Different sensitivity analysis techniques are available for this stage. Typically, they can be divided in local and global sensitivity analyses. Local sensitivity analyses investigate how the design varies for a small change of the model parameters. Since some model parameters considered in this research have high uncertainties, a local sensitivity analysis would not explore the full model parameter space and not capture the non-linearity of the model. A global approach is then considered. In particular, it is studied how the model parameters uncertainties influence the design outputs uncertainties. The aim of the global sensitivity analysis is to fully explore the model parameter space and study the consequences on the design of innovations and design decisions. This is explained in detail in Section 2.2.

The reader can find an example and more detailed descriptions of the methods in Chapter 4 of [12].

2.1. Optimization problem

A generic optimization problem can be formulated as:

$$\begin{aligned} \underset{\boldsymbol{x}}{\text{minimize}} \quad & f(\boldsymbol{x}) \\ \text{subject to} \quad & \boldsymbol{l} \le \boldsymbol{x} \le \boldsymbol{u} \\ & \boldsymbol{g}(\boldsymbol{x}) \le 0 \\ & \boldsymbol{h}(\boldsymbol{x}) = 0 \end{aligned} \tag{1}$$

Where $\boldsymbol{x}$ are the design variables, f the objective function, $\boldsymbol{l}$ and $\boldsymbol{u}$ the lower and upper bounds of $\boldsymbol{x}$, $\boldsymbol{g}$ the inequality constraints and $\boldsymbol{h}$ the equality constraints.

A gradient-based algorithm, in particular Sequential Quadratic Programming (*SQP*), is used in this work because it is known to be efficient, robust and accurate for continuous optimization problems of the sizes considered in this work. The MATLAB function *fmincon* [17] is used.

One way to study the optimal design locally, is to look at the Lagrange multipliers of the solution (Post-optimal sensitivity analysis). For a solution to be optimal, the *KKT* (Karush–Kuhn–Tucker) conditions [18] must be satisfied:

$$\begin{gathered}\nabla f + \nabla \boldsymbol{g}\boldsymbol{\lambda}_i + \nabla \boldsymbol{h}\boldsymbol{\lambda}_e = \mathbf{0} \\ \boldsymbol{g}(\mathbf{0}) \leq \mathbf{0} \\ \boldsymbol{g}(\mathbf{0})\boldsymbol{\lambda}_i = \mathbf{0} \\ \boldsymbol{\lambda}_i \geq \mathbf{0}\end{gathered} \tag{2}$$

Where $\boldsymbol{\lambda}_i$ are the Lagrange multipliers of the inequality constraints and $\boldsymbol{\lambda}_e$ of the equality.

Lagrange multipliers indicate how much the objective function varies with a small change of a given constraint limit. They can be approximated as the partial derivative of the objective function with respect to the constraint:

$$\lambda_j \approx \frac{\partial f}{\partial g_j} \tag{3}$$

Lagrange multipliers are therefore representative of the constraint strength. A comparison between Lagrange multipliers can be informative on the design, showing which constraint is design driver. To allow for a meaningful comparison between Lagrange multipliers, they should be normalized with the constraint value. In this way, Lagrange multipliers indicate how much a relative variation of the constraint limit influences the objective function. The largest relative Lagrange multiplier has the largest influence on the design. Small changes in the associated constraint limit would yield a larger change in the objective function. Thus, these large values indicate constraints that deserve extra attention in terms of both accuracy of the estimation of the constraint limit and for prioritizing technological development. These constraint types can be considered strong. On the contrary, a small Lagrange multiplier indicates that the objective function would decrease a small quantity with a change of the constraint value (*i.e.* the constraint is preventing the optimizer from finding a slightly improved design). These constraint types can be considered weak. When a Lagrange multiplier is zero, the relative constraint is not active.

2.2. Global sensitivity analysis

The global sensitivity presented in this section is used to study how the uncertainties propagate throughout a model. To perform this analysis, the MATLAB toolbox *UQLab* [19] is used.

In Figure 2, a graphical representation of the framework to perform a global sensitivity analysis is shown. In this work, the computational model (*Step A*) is the optimization problem.

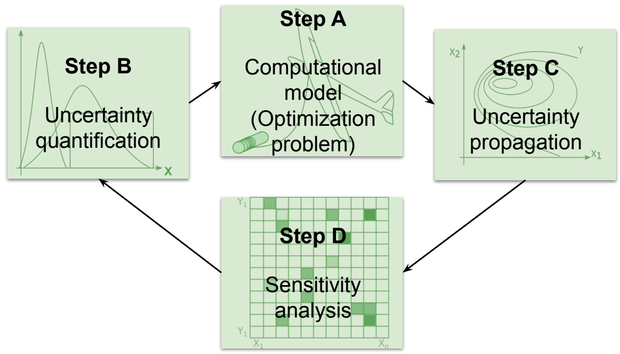

Figure 2: The general uncertainty quantification framework .

2.2.1. Uncertainty Quantification

The uncertainty quantification represents *Step B* in Figure 2. In this step, the uncertainty sources and the relative uncertainties are to be evaluated.
This step has many applications. The first application is to represent aleatory uncertainties, also known as statistical uncertainties. These uncertainties are related to random processes.
The second application is to represent epistemic uncertainties, also known as systematic uncertainties. These uncertainties are related to parameters that in principle could be known, but at the current stage they are not. In preliminary studies, such as the one presented in this paper, they are of particular interest because they allow to quantify the impact of these parameters on the design process and the final design.
During the modelling phase, to assign an epistemic uncertainty is useful to understand whenever an approximate model of a subsystem is adequate or more development in the modelling is needed.
During the design phase, the performance of a component can be modelled with an epistemic uncertainty. If the component performance is relevant for the final output, then an accurate design is justified.
During preliminary studies, an epistemic uncertainty can model the technological development of a component. If the improvement of a component performance leads to a large benefit for the system, research and development of that component is justified.

2.2.2. Uncertainty propagation & surrogate models

Once the uncertainty sources are identified and quantified, it should be studied how they propagate throughout the model (Step C in Figure 2). Many techniques are available for this step, Monte Carlo Simulation [20] is among the most commonly used. This technique requires a high number of model evaluations (the optimization problem in this case), so it is not selected for this study.

There exist other methods which use a smaller number of model evaluations compared to Monte Carlo Simulation (about 2-3 order of magnitude of difference [21]) to fit the model behaviour with a surrogate model. A surrogate model, also known as meta-model, is a function that fits the real model. Typically, evaluating surrogate models have negligible computational cost compared to the real model.

The process of creation of surrogate models consists of two steps: the sampling and the fitting.

First, the model is evaluated in many points in the model parameter space, according to the model parameters uncertainties. To reduce the number of evaluations, some techniques are available to chose the evaluation points. The most common are *Latin hypercube sampling*, known for its attractive space filling property, and *quasi-random sequences* [21]. In the present work *Latin hypercube sampling* is used. Since the evaluations are independent, the evaluations can be computed in parallel.

Second, the functional form of the surrogate model must be selected. Common shapes are *Polynomial chaos expansions*, *Low-rank tensor approximations*, *Kriging (a.k.a Gaussian processes)* and *Support vector machines*. In this work *Polynomial chaos expansions*, which consists in a polynomial approximation made of multivariate orthogonal polynomials [21], is used.

2.2.3. Evaluation of statistics over the model parameter space

The evaluations carried out for the creation of the meta-models can also be studied with a statistical approach. One could consider mean and variance of these evaluations.

The mean of the optimal outputs represent the expected optimal design. It can be interpreted as the centre of the design space. The standard deviations of the outputs is an indication of sensitivity to uncertainties. Outputs with large standard deviations with respect to the mean are sensitive to the model parameter uncertainties and thus it should be understood how they change in the model parameters space.

The statistics of the Lagrange multipliers statistics help to identify how constraints drive the design in the parameter space. A constraint is rarely design driving when its Lagrange multiplier has low mean and low standard deviation. A Lagrange multiplier with high mean and low variance represents a constraint that is almost always active and strong. A Lagrange multiplier with high mean and high standard deviation shows that the constraint can be important for some uncertain parameters combinations, and not relevant for other combinations.

2.2.4. Variance based sensitivity analysis

Once the surrogate models are evaluated, the sensitivity analysis can be finalized. In this work a *variance based decomposition* is used to quantify how the outputs variance is influenced by each model parameter variance. Given an input vector with mutually independent variables $\mathbf{X} = (X_1, \ldots, X_d)$ (the model parameters in this work), a deterministic model f (a surrogate model in this work), and the output $Y = f(\mathbf{X})$ (a surrogate model evaluation in this work), the output variance can be decomposed as [22]:

$$\mathrm{Var}(Y) = \sum_{i=1}^{d} D_i(Y) + \sum_{i<j}^{d} D_{ij}(Y) + \cdots + D_{12\ldots d}(Y) \tag{4}$$

where $D_i(Y)$ represents the variance of the expected value of Y, given X_i: $D_i(Y) = \mathrm{Var}\left[\mathbb{E}\left(Y|X_i\right)\right]$, $D_{ij}(Y) = \mathrm{Var}\left[\mathbb{E}\left(Y|X_i, X_j\right)\right] - D_i(Y) - D_j(Y)$ and so on for higher order interactions. The so-called *Sobol indices* or *variance based sensitivity indices* [22] are computed as:

$$S_i = \frac{D_i(Y)}{\mathrm{Var}(Y)}, \quad S_{ij} = \frac{D_{ij}(Y)}{\mathrm{Var}(Y)}, \quad \ldots \tag{5}$$

The total Sobol indices are used in this work, they are:

$$S_{T_i} = S_i + \sum_{i<j} S_{ij} + \sum_{j\neq i, k\neq i, j<k} S_{ijk} + \ldots = \sum_{l \in \# i} S_l \tag{6}$$

The total Sobol indices indicate how much of the output variance is is due to model parameter X_i variance, considering its interactions with all the other model parameters. This is similar to the local sensitivity one obtains with gradients, however, by looking at the variance of the output across the whole parameter space, it gives a more global indication of sensitivity. A high Sobol index indicates that a given parameter has a strong influence over the output globally.

Table 1: Dimension, units and description of the design variables. n represents the number of wind speeds between cut-in and cut-out considered in the design.

	Dim	Units	Description
s	1x1	m	Kite wing span
AR	1x1	-	Kite wing aspect ratio
d_t	1x1	m	Tether diameter
l_t	1x1	m	Tether length
α_{TO}	1x1	rad	Climbing angle during the take-off
β	1x1	rad	Elevation angle
V_{in}	1x1	m/s	Cut-in wind speed
V_{out}	1x1	m/s	Cut-out wind speed
Q_{turb}	1x1	-	Percentage of the thrust given by the on-board turbine during the take-off
t_A	1x1	m	Spar cap thickness close to the tip
t_B	1x1	m	Spar cap thickness at half way between tip and tether attachment
t_C	1x1	m	Spar cap thickness at the tether attachment and inward
x_a	1x1	m	Spanwise position of the tether attachment
C_L	1xn	-	Lift coefficient of the kite
γ_t	1xn	-	Coefficient of drag corresponding to on-board production
γ_{out}	1xn	-	Reel-out velocity coefficient
γ_{in}	1xn	-	Reel-in velocity coefficient

3. Annual energy production maximization

In this section, *AWES* designs aiming to maximize the *AEP* are studied. The unified model [13] is implemented in *MATLAB*, in order to be coupled with an optimization algorithm.

3.1. Problem formulation

The selected design variables are presented in Table 1. Some describe the system geometry and the structural design. Most of them are performance parameters, that will drive a more accurate design in the future.

The inequality constraints included in the optimization are related to the tether strength $\tilde{\sigma_{lim}}$ (with the related safety factor $SF_{\sigma\ lim}$) , the rated power P_{rated}, the minimum operational altitude h_{min}, the maximum tip deflection

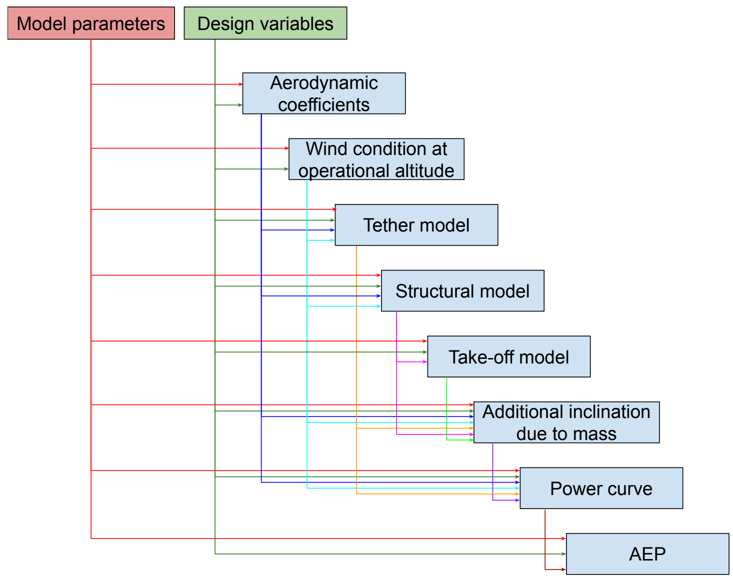

Figure 3: Flowchart of the physical model implementation.

δ_{max} and the structural material strength $\tilde{\sigma}_{str}$:

$$\boldsymbol{g}(\boldsymbol{x}) = \begin{pmatrix} \sigma - \frac{\tilde{\sigma_{lim}}}{SF_{\sigma\ lim}} \\ P - P_{rated} \\ h_{min} - h \\ \delta - \delta_{max} \\ \sigma_{str} - \tilde{\sigma}_{str} \end{pmatrix} \leq \boldsymbol{0} \tag{7}$$

The equality constraint is related to the kite wing area:

$$h(\boldsymbol{x}) = \frac{s^2}{AR} - A_{kite} = 0 \tag{8}$$

The Annual Energy Production AEP minus the energy spent to take off, with the assumption of one take-off a day, is the objective function.
In Figure 3, the flowchart of the code is presented. The optimizer modifies the design variables to maximize the AEP. The model [13] can handle power generation at the ground and on-board at the same time. Therefore, the optimizer designs a hybrid $AWES$ to maximizes the AEP. The aim of this study is to look at the optimum $AWES$ and to define the common physical characteristics between *Fly-Gen* and *Ground-Gen* $AWESs$.
The model is composed of only analytic equations [13], allowing for a extremely fast evaluation of the design.

Table 2: Main results of the optimization example for the AEP maximization case.

AEP	16.5	GWh
CF	63.0	%
m_{tot}	6646	kg
l_t	825	m
d_t	34	mm
h	277	m
β	20	°
s	63.7	m
AR	33.8	-
A_{turb}	10	m^2
A_{prop}	0	m^2
α_{TO}	8	°
λ_{te}	1.3	GWh/ -
λ_{CL}	2.5	GWh/-

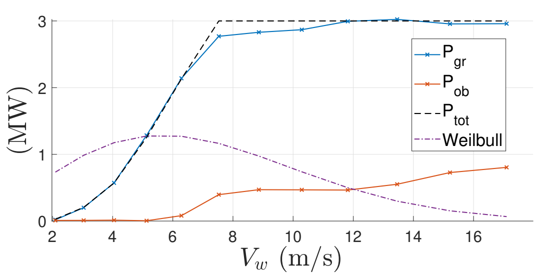

Figure 4: Power ground generated (P_{gr}), power on-board generated (P_{ob}) and power output (P_{tot}) for the *AWES* optimization example.

3.2. Example of an AWES optimization

The results of one optimization with the model parameters (Table 3) set to the mean values are shown.

Part of the power is generated on-board and part on the ground (red and blue lines respectively in Figure 4). The total power curve of the system, which includes also the power spent during the reel-in phase, is reaching the rated power at about 7 m/s. In Table 2, the main outputs are listed.

The system produces 16.5 GWh in one year, corresponding to a capacity factor of 63 %. The tether stress, shown in Figure 5a reaches the maximum from about 5 to 8 m/s, which results in a linear trend for the power as

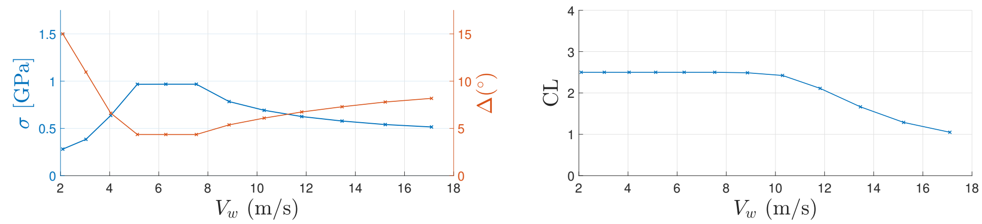

(a) (b)

Figure 5: Tether stress σ and additional inclination due to gravitational force Δ (a) and lift coefficient (b) as function of wind speed for the *AWES* optimization example.

function of wind speed in this range. The total flying mass m_{tot} influences the additional inclination angle due to gravity Δ, making it large at low wind speeds. The total flying mass m_{tot} is composed of the kite structural mass, the additional on-board mass and half of the tether mass. This mass is used to evaluate Δ [13]. It can be proven analytically [13] that when σ is constant, Δ will be too.

The lift coefficient (Figure 5b) is set to the maximum until rated power is reached. After this, it is lowered to decrease the glide ratio and the kite speed.

The operational altitude is higher than the hub height of conventional wind turbines of the same rated power. An aspect ratio of 33.8 is chosen, showing that an extremely slender wing is optimal. The on-board turbines provide the thrust needed to take-off (the area of additional propellers A_{prop} is zero): the configurations with propeller mass not useful for the power generation are discarded. The Lagrange multiplier of the tether strength λ_{te} shows that an improvement of 1% of this constraint results in an *AEP* increase of 13 MWh. An improvement of 1 % in $C_{L\,max}$ ($C_{L\,max} = 2.525$) results in an *AEP* increase of 25 MWh. For the same relative change in the constraint limit, an increase in maximum lift coefficient brings more benefit than an increase in tether strength. Thus, the constraint on the maximum lift coefficient is considered stronger than the constraint on the tether strength.

3.3. Algorithm validation

Two tests have been carried out to validate the algorithm.

The first is a test to understand if the problem is well posed. One model parameter, expected to strongly influence the objective function, is incrementally modified and the optimization problem is solved for each increment. To make sure a global minimum is found for each increment, a number of optimization problems with different initial conditions are solved and the best, in term of objective function, is considered a global optimum. The objective function of the converged solutions, if plotted against the selected model parameter, should be a continuous and smooth function. This test is also used to estimate that 10 optimization problems with different initial conditions have to converge to have a good estimation of the global minimum.

The second test is a benchmark with literature results. The verification is based on two commercial designs, where only part of the design and performance are published. Since not all the information is available, all parameters available in literature are set to reference values, the unknown parameters are set to reasonable/estimated values. The objective function is modified to be the difference between the literature power curve and the optimization output. The scope of the validation is not to replicate the selected prototypes, as they are the result of an iterative design process which may not lead to the same result of the optimization proposed in this work. The scope of the validation is instead to check if the optimization brings to reasonable designs.

For the *Ground-Gen* validation, the second prototype *AP2* of the company *Ampyx Power* [7] is used as a reference. The reference power curve is found in [23], and the reference parameters in a previous work from the same author [24]. The reference power curve is validated with the experimental data [25]. In Figure 6, the reference power curve and the optimization output are shown in the top plot. In the bottom plot, the reel-out tension force acting on the tether is found to be almost constant during operation and the reel-out coefficient γ_{out} is slightly lower than optimal value of 1/3.

For the *Fly-Gen* validation, the *Wing 7* from *Makani Power* [26] is used as a reference. The reference parameters are taken from Table 28.8 of the book: *Airborne Wind Energy 2013* [1] and in [27, 28]. All the four regions (maintenance of flight, generation, tension constrained generation, maximum power) highlighted by Vander Lind [26] can be spotted in the plots given in Figure 7.

The design variables and the outputs trends are considered reasonable. More plots and outputs of the validation can be found in Section 5.3 of [12].

3.4. Uncertainty quantification

A system with a rated power of 3 MW is selected as a study case. Twenty parameters, considered as potential design drivers, are chosen to be studied

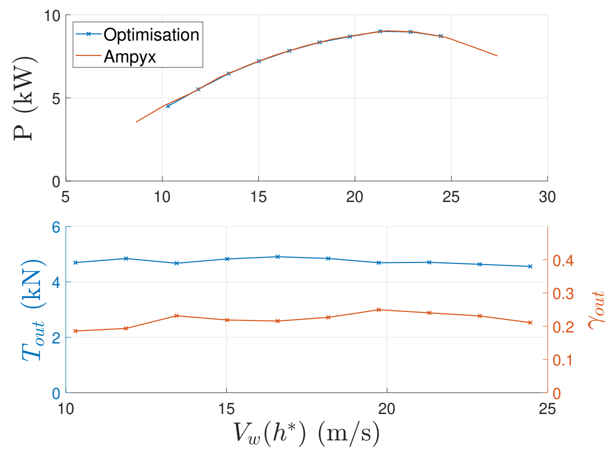

Figure 6: Relevant plots for the *Ground-Gen* validation. On the top plot, the reference power curve and the optimisation output are plotted as function of the wind speed at operational altitude. On the lower plot, the reel-out coefficient and the reel-out force are shown.

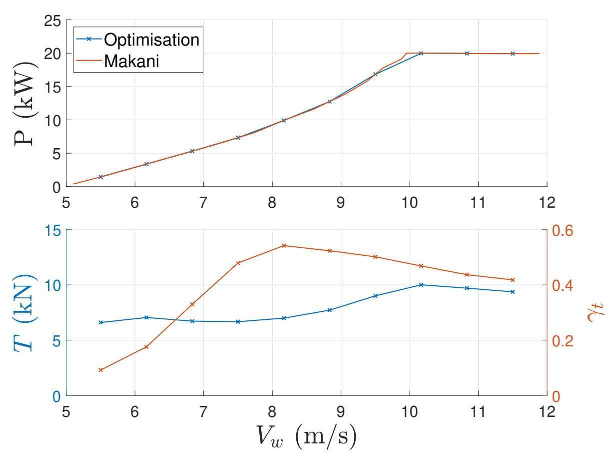

Figure 7: Relevant plots for the *Fly-Gen* validation. On the top plot, the reference power curve and the optimisation outputs are shown. On the bottom, the tether force and the coefficient of power generation are shown.

Table 3: Model parameters uncertainties and descriptions for the AEP maximization case. For detailed explanation see [13].

par	Min	Max	Units	Description
$SF_{\sigma\ lim}$	1.1	2	-	Safety factor on the tether strength. The tether strength is 1.5 GPa.
C_{D0}	0.01	0.1	-	Drag coefficient at zero lift.
$C_{\perp}$	0.6	1.2	-	Tether drag coefficient.
$C_{L\ max}$	1	4	-	Upper bound of the lift coefficient design variables (C_L).
η_{out}	0.75	0.9	-	Efficiency of reel-out phase.
η_t	0.7	0.85	-	Efficiency of the on-board generation.
η_{in}	0.3	0.85	-	Efficiency of reel-in.
$\eta_{t\ pr}$	0.5	0.7	-	Efficiency of the turbines used in propeller mode with respect to disc theory.
η_{pr}	0.7	0.9	-	Efficiency of the propellers with respect to disc theory.
η_d	0.8	0.95	-	Minimum efficiency due to induction factor of the on-board turbines.
V	2	40	kV	Line voltage in the tether.
E_{gen}	2.5	16	kW/kg	Power density of the motor/generators[a].
ρ_{wing}	1400	2200	kg/m^3	Structural material density.
f_{wing}	0	3	-	f_{wing} times the spar caps mass models the structural material not included in the wing model.
δ_{max}	1	10	%	Percentage of the span: maximum tip and central displacement.
h_{min}	150	250	m	Minimum allowed operational altitude.
A_{kite}	80	160	m^2	Kite wing area.
α	0.1	0.3	-	Wind shear coefficient.
k	1	3	-	Weibull form parameter.
A	6	15	m/s	Weibull scale parameter.

[a]The reference literature value is 2500 W/kg [29], new technologies could bring this value up to 16000 W/kg [30].

with a *variance based decomposition* analysis. The model parameters and the assigned uncertainties are listed in Table 3.

3.5. Global sensitivity analysis results

Given the uncertainties in Table 3, the global sensitivity analysis is carried out. To estimate how many evaluations are needed for having converged Sobol indices, three global sensitivity analyses are carried out with increasing number of evaluations and a total number of 600 evaluations are chosen. Each evaluation is selected within 10 converged optimization problems starting from different initial conditions, to avoid local minimums.

Figures 8 shows the total Sobol indices. On the extreme right of the figure, the mean and the standard deviation of the investigated outputs are shown. A dark color highlights a high dependence between the output variance and the input variance.

For the considered uncertainties, the mean capacity factor is of 63.6 %, higher than typical values of conventional wind turbines (25 to 45 %). Its variance is mainly influenced by the drag coefficient at zero lift C_{D0}, the maximum lift coefficient $C_{L\,max}$ and the two Weibull parameters, describing the wind resources.

To graphically interpret the results of the *variance based decomposition*, one could plot the meta-models created for the uncertainty propagation step (see Section 2.2.2 for details).

Figure 9a shows how the capacity factor CF varies as function of $C_{L\,max}$ and C_{D0}. Small C_{D0} with relative low $C_{L\,max}$ can give high capacity factors, for higher C_{D0} the same power output is attained with way higher lift coefficients. This shows that the aerodynamic design should be performed considering drag and lift at the same time and not only lift.

Figure 9b is instead showing how CF varies according to the Weibull parameters. Clearly, regions with high wind resources allow extremely high capacity factors.

The reader should note that the Sobol indices depend greatly on the assumed uncertainty of the inputs. If an input parameter uncertainty was doubled, one would expect the Sobol index for that parameter to be larger, while the other indices would become smaller. Taking the capacity factor as an example, reducing the uncertainty of the Weibull scale parameter would show a lower importance of that input but also an increased importance for $C_{L\,max}$ and C_{D0}. However, the Sobol analysis is used to help identify important design trends that are subsequently showed in the meta-model plots. Changing the

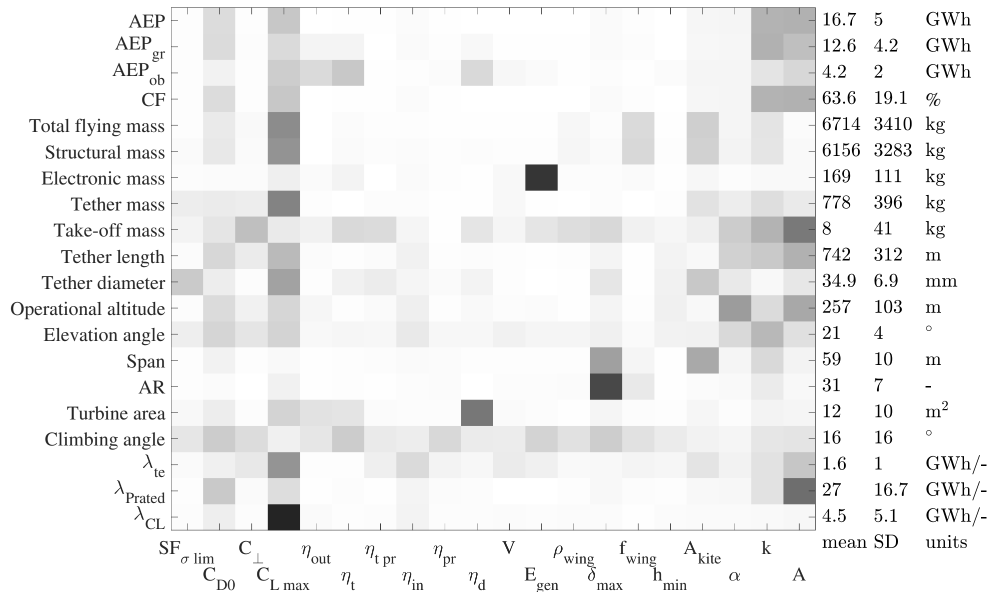

Figure 8: Graphical visualization of the total Sobol indices and output statistics for the AEP maximization.

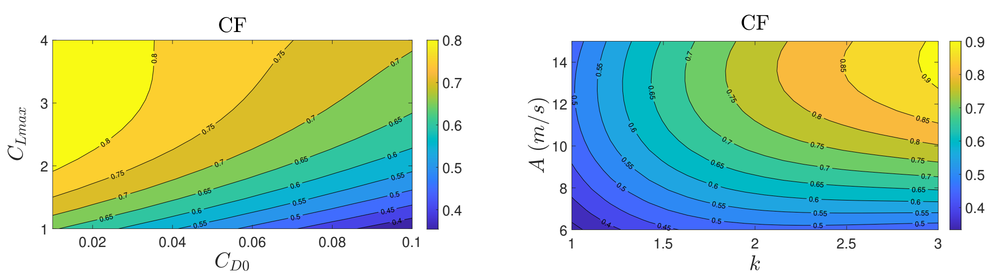

(a)

(b)

Figure 9: Meta-model of the capacity factor as function of the drag coefficient at zero lift C_{D0} and the maximum lift coefficient $C_{L\ max}$ (a) and as function of the Weibull form parameter k and the Weibull scale parameter A (b).

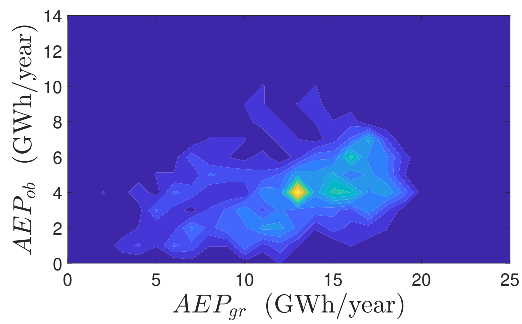

Figure 10: Evaluations density of the annual energy production generated on the ground (AEP_{gr}) and on-board (AEP_{ob}).

uncertainties is expected to not affect the design trends shown in the meta model significantly. So despite the subjective input uncertainty assumptions, the important conclusions from this analysis should not be effected greatly from these assumptions.

The power is mainly ground generated AEP_{gr} and the variance of power ground and on-board generated is additionally influenced by the efficiencies of reel-out η_{out} and on-board generation η_t.

In Figure 10, the evaluation density of the two annual productions types is shown. All the evaluations are characterized by the coexistence of two generation types. From a physical point of view, it is optimum to have on-board wind turbines big enough to take off and use these during the generation phase. Indeed, the take-off mass (mass only used during the take-off) has a really low mean value if compared with the electronics mass mean.

The variance of parameters with low Sobol indices have little influence on the output variance compared with other parameters. For example, the safety factor on the tether material strength $SF_{\sigma\ lim}$ variance has almost no influence on the AEP variance. During the design phase, $SF_{\sigma\ lim}$ can be set to high values and a kite with high AEP can still be designed by varying the other parameters associated with high Sobol indices. Similar considerations apply to the other parameters associated with low Sobol indices.

Mass related quantities show the structural design characteristics. The total flying mass has an average mass of about 6.7 tonne, with a high standard deviation. The structural mass variance is mainly influenced by kite aerodynamic coefficients, the wing area and the mass parameter f_{wing}.

Wind conditions and the kite aerodynamics strongly influence tether length

and mass and the operational altitude variances: the optimizer tries to increase the operational altitude to reach improved wind resources. The tether diameter variance depends on the tether safety factor $SF_{\sigma\, lim}$, the wing area A_{kite} and the maximum lift coefficient: the last two parameters influence the thrust force and therefore the stress on the tether.
The elevation angle has an average of 21.2° and its variance is influenced by the wind conditions and kite aerodynamics. The optimizer tries to reach the improved wind resources available at high altitudes.
The wing span s and aspect ratio AR combine to give the wing area A_{kite}. The aspect ratio AR variance is mainly influenced by the maximum structure deflection δ_{max}, the span by δ_{max} and A_{kite}. The average structural mass density is of 51 kg/m^2, higher than typical values for gliders (approximately between 10 and 25 kg/m^2 [31]).
The on-board turbine rotor area variance is directly influenced by the mean efficiency due to disc theory η_d.
As the take-off is performed with the on-board wind turbine used in propeller mode, the take off sub-system design (take-off mass and climbing angle) has no clear dependence. The mean value of the climbing angle suggests that in most of the cases a linear take-off is chosen.
The last three rows in Figure 8 are related to the three Lagrange multipliers with high values: the Lagrange multiplier of the tether strength constraint λ_{te}, on the rated power λ_{Prated} and on the maximum lift coefficient λ_{CL}.
The Lagrange multiplier of the tether strength constraint is mainly influenced by the kite and tether aerodynamics and the wind conditions. Interestingly, the Lagrange multiplier on the tether strength variance is almost not influenced by the safety factor on the tether strength itself. A change on the safety factor does not impact the constraint strength as much as a change of a high Sobol index parameter (for instance maximum lift coefficient). To make the constraint on the tether strength weaker, the easiest approach is to modify the kite aerodynamics and not to have a stronger tether. Thus, one can employ high safety factors to improve the safety and reliability of *AWES*, while still having good power production performances.
The Sobol indices of the Lagrange multipliers on the rated power show that in windy regions this constraint is stronger and it would be beneficial to increase the rated power (*i.e.* the generator size) for the same system.
Figure 11 shows the meta-model of the Lagrange multiplier of the lift coefficient limit as function of the maximum lift coefficient itself and the drag coefficient at zero lift. λ_{CL} represents the the constraint strength or, in other

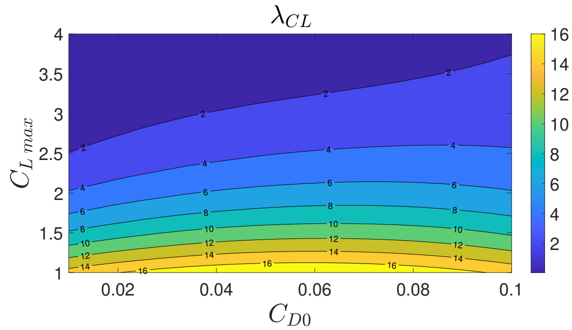

Figure 11: Meta-model of the Lagrange multiplier of the maximum lift coefficient as function of the drag coefficient at zero lift C_{D0} and the maximum lift coefficient $C_{L\,max}$.

words, the increase in the objective function (AEP) for a relative small increase in the constraint limit ($C_{L\,max}$). This constraint is stronger when the upper bound itself $C_{L\,max}$ is low. On the contrary, for high $C_{L\,max}$ this constrain is basically not active.

According to these results, a extremely high maximum lift coefficient $C_{L\,max}$ has reduced benefits for the annual energy production. λ_{CL} is not influenced by the structural material density variance and the variance of the mass parameter f_{wing}. These two parameters variances represent different aircraft designs that aim to lower the flying mass. This shows that using lighter or heavier materials does not strongly influence the aerodynamic design.

3.6. Discussion

For the given uncertainties, the design of a crosswind *AWES* aiming to maximize the power production is highly dependent on the kite aerodynamics. An *AWES* designer, when designing for a chosen capacity factor, could take conservative values of the parameters associated with small Sobol indices and design according to the parameters associated with large Sobol indices. In such a way, a preliminary design can be realized and afterwards a more detailed design of all the subsystems can be performed, obtaining robust designs. For instance, one could initially assume a low efficiency of power generation (low Sobol index parameter) and perform a preliminary design by choosing the kite aerodynamic shape and the dimension (high Sobol index parameters related to the kite design) targeting the given capacity factor. At this stage, an accurate value of the efficiency can be evaluated.

To maximize the capacity factor, one must consider both the aerodynamic lift

and drag. Good solutions range between extremely low drag with moderate lift levels, to higher drag and corresponding higher lift. When designing the aerodynamics, an increase in lift with a correspondent high increase in drag is generally not justified.
The structural design of the kite, (*i.e.* the structural mass, electronic mass, span and aspect ratio), is not strongly influenced by the wind conditions. This means that the same kite design would be close to optimal in a wide range of wind conditions. Therefore, large wing area kites - designed with the same features as smaller kites - could be placed in low wind regions, to obtain high capacity factors.
Concerning safety and regulation, the minimum operational altitude and the safety factor on the tether strength have a small impact on the capacity factor. If in the future some regulations will constrain these quantities, *AWESs* can still be designed to have a high capacity factor.
In Table 4, some characteristics of a convectional wind turbine of 3.4 MW of rated power are introduced (IEA-3.4-130 [32]). Given the similar rated power, a comparison between this wind turbine and the designs presented in this section can be performed. The operational altitude of *AWESs* is approximately the double of the wind turbine hub height. The structural wing mass compared with the rotor mass (three times the blade mass) is approximately 12 %. The tower for wind turbines has the same role of the tether for *AWESs*: they transmit the thrust force needed for the power generation to the ground. The tether mass is three orders of magnitudes smaller than the tower mass. These few considerations confirm the radical differences between *AWESs* and conventional wind turbine technology.

4. Profit maximization

In this section, the cost model presented in [13] is included into the optimization, to evaluate designs aiming to be economically profitable. It should be noted that the economic model has not been validated, but it can be used for comparative studies between the *Ground-Gen* and *Fly-Gen AWESs*.

4.1. Problem formulation

The same design variables presented in Table 1 are used in this case, with some differences. First, the tower height is added as a design variable, second the wing area is not constrained, so that the optimizer can pick the optimal wing area according to economic considerations.

Table 4: Summary of the configuration of the 3.4-MW land-based wind turbine (IEA-3.4-130 [32].

Rated aerodynamic power	3.60	MW
Hub height	110.0	m
Blade mass	16441	kg
Blade cost	121	k$
Aerodynamic AEP	14.99	GWh
ICC	4142	k$
Rated electrical power	3.37	MW
Rotor diameter	130.0	m
Tower mass	553	ton
Tower cost	829.7	k$
Electrical AEP	13.94	GWh
LCOE	44.18	$/MWh

The objective function is the annual profit:

$$\Pi = p_{el} \cdot AEP - (ICC \cdot CRF + OMC) \tag{9}$$

Where the average price of electricity p_{el} times the annual energy production AEP represents the annual revenues and the term in the brackets represents the annual costs. ICC stands for Initial Capital Cost, CRF for Capital Recovery Factor (see [13]) and OMC for Operational and Maintenance Costs. With this formulation, p_{el} is the weight between revenues ($p_{el} \cdot AEP$) and costs ($ICC \cdot CRF + OMC$).

Gradient based optimization is still used to solve the design problem. Since the cost function is not always continuous between ground and flight generation, the generation type is no longer part of the optimization and it is chosen *a-priori*.

The physical model shown in Figure 3 is used here. However, for the operational altitude computation, the tower height is included. The initial capital cost and the operation costs are evaluated with the model presented in [13].

4.2. Uncertainty quantification

The uncertain parameters uncertainties related to the physical model shown in Table 3 are included in the uncertainty quantification. In addition, the uncertainties related to the cost model [13] are considered. Epistemic uncertainties related to rated power, number of operational years, maximum

Table 5: Model parameters uncertainties and descriptions for the economic analysis. The first parameters group has a uniform distribution, the second a Gaussian distribution. For detailed explanation of the parameters see [13].

par	Min	Max	Units	Description
p_{wing}	20	200	€/kg	Price per unit mass of the structural material of the aircraft.
f_{te}	1.2	2	-	Cable manufacturing additional price in case of both structural and electrical components.
p_{Ag}	20	200	€/m^2	Price per unit area of the launch and landing system cost.
f_{tw}	1	3	-	Coefficient for the manufacturing of the tower.
$f_{r\,kite}$	0	0.5	-	Number of kite replacement in one year.
$f_{el\,FG}$	1.2	1.8	-	Factor for the on-board electronic cost.
h_{tw}	150	250	m	Maximum tower height.
n_y	15	25	-	Number of operational years.
P_r	1.5	4.5	MW	Rated power.
par	Mean	SD	Units	Description
p_{te}	200	50	€/kg	Price per unit mass of the structural material of the cable.
a_{gen}	1.2	0.2	€/MW	Coefficient for the generator cost.
C_{fix}	150	80	k€	Fix cost.
OC	9	3	€/MWh	Operation costs.
i	0.09	0.015	-	Discount rate [33].
p_{el}	40	10	€/MWh	Price of electricity [34].

Table 6: Main outputs of the *Ground-Gen AWES* optimization example.

$LCOE$	23	€/MWh
ICC	1934	k€
OMC	210	k€/year
AEP	17.8	GWh
CF	68.0	%
$C_{structure}$	134	k€
C_{tether}	106	k€
$C_{electronics}$	1063	k€
C_{TO}	327	k€
C_{tower}	136	k€
C_{fix}	169	k€
m_{tot}	1679	kg
l_t	602	m
d_t	42	mm
Tower height	125	m
β	20	°
s	59	m
AR	12	-
life_{te}	8.3	years

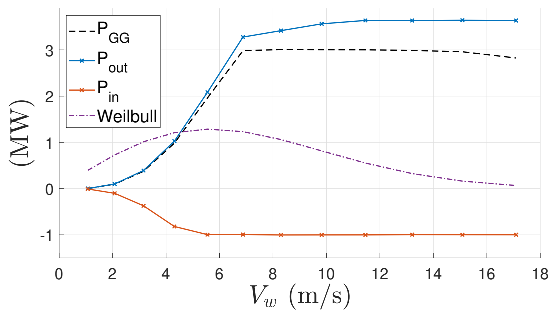

Figure 12: Mean power production P_{GG}, power produced during the reel-out phase P_{out} and reel-in phase P_{in} for the *Ground-Gen AWES* example.

tower height and frequency of kite replacement are also included. In particular, the frequency of kite replacement is due to the frequency of control failures leading to a crash and other related operational faults. The additional uncertainties are summarized in Table 5.

4.3. Example of a Ground-Gen AWES optimization

The results of the optimization of a *Ground-Gen* with the model parameters set to mean values are analyzed. In Figure 12 the mean power production and the power spent during the reel-in and reel-out is shown.

The main outputs are given in Table 6. The system has a *LCOE* of 23 €/MWh. Most of the initial capital cost is related to the electronics. A wing area of 295 m^2 is found to be optimal, along with a span of 59 m and an aspect ratio of 12. The relatively low aspect ratio gives a large airfoil absolute thickness, which in-turn increases the stiffness leading to a cheaper and low relative mass. The rated power is reached at around 7 m/s, leading to an extremely high capacity factor.

In Figure 13a, the lift coefficient and the tether stress as function of wind speed are shown. The tether stress leads to an operational life of 8.3 years for the tether itself. The operational life due to creep is computed by using the Miner'Rule on the creep curves for DM20 given in [35]. The maximum lift coefficient is kept constant below rated conditions and then reduced to maintain constant power.

In Figure 13b, the reel-out coefficient γ_{out} and the additional inclination due to mass Δ are shown. At low wind speed, the optimizer reduces γ_{out} to increase the kite speed and thus the aerodynamic forces. In this way, Δ and

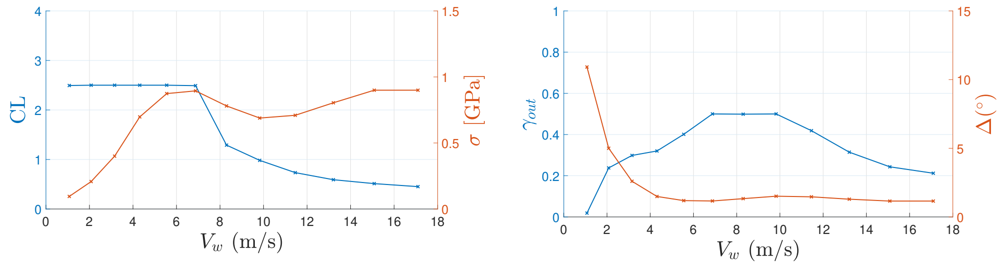

(a) (b)

Figure 13: Lift coefficient and tether stress (a); reel-out coefficient γ_{out} and additional inclination due to gravitational force Δ (b) as function of wind speed for the *Ground-Gen AWES* example.

the related power losses due to gravitational forces, can be contained within reasonable limits.

4.4. Global sensitivity analysis results for Ground-Gen

The results of the global sensitivity analysis carried out on *Ground-Gen* are now presented. 2000 points are considered a sufficient number to have a good representation of the model parameter space and to build a meta-model. Each of these points is the best (in term of objective function) of 7 converged optimization problems run with random initial conditions.
In Figure A.20 a graphical representation of the total Sobol indices and of the evaluations statistics are given.
The designs have a positive mean annual profit, meaning that a *Ground-Gen* can be attractive from an investment point of view. However, the standard deviation of the profit is high compared to the mean: some designs may not be profitable and some others are much more attractive than the average. The total Sobol indices highlight that the profit variance depends mainly on the electricity price p_{el} variance and on the rated power P_r variance. This is an important finding for policy makers. To finance the significant research and development of *AWES*, investors want high expectation of profit, with low risk. Thus, policy makers could make sure that a minimum price of electricity will be paid for green energy produced by *AWES*. In this way, investors are sure to have high profits. Investors should also notice that high capacity factors imply power generation with low wind conditions. In countries where wind energy have a big share of the energy market, the hours with low wind speeds have high electricity price. Thus, power fed into

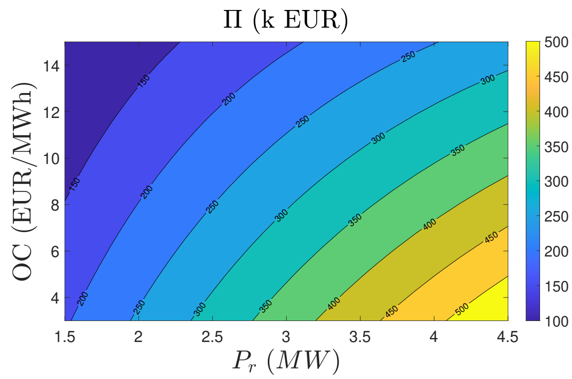

Figure 14: Meta-model of the annual profit as function of the rated power P_r and of the operational costs OC.

the grid in these hours is extra profitable. The meta-model of the profit as function of P_r and the operational costs OC is shown in Figure 14. It is clear that low operational costs improve the profits. Interestingly, the increase of rated power corresponds to a profit increase: the up-scaling of *Ground-Gen AWESs* is profitable.

The average $LCOE$ is approximately 25 €/MWh, with a relatively small variance. $LCOE$ variance is mainly influenced by the variance on the operational costs, the wind resources and the kite aerodynamics. The optimal capacity factors has an average of 57 %, higher than typical capacity factors for conventional wind turbines.

By analyzing the average cost breakdown of the initial capital cost over the model parameter space, the highest cost is due to the electronics (60 %), followed by take-off structure costs (12 %), fix costs (10 %) and tether (8 %). The kite structure cost (5 %) is generally low, if compared with the other subsystems. This points out that for *Ground-Gen AWESs*, it is optimum to operate large kites for given generator size, so that the capacity factor is large.

The mass of the structure, take-off subsystem and tether have high uncertainties. The structural mass uncertainty depends on the uncertainties related to the structural model (represented by f_{wing}), the material price p_{wing}, the frequency of kite replacement $f_{r\ kite}$, rated power P_r, electricity price p_{el} and the wind resources (k and A). The dependence on the frequency of kite replacement uncertainty highlights that, if the kite needs to be replaced often due to crashes, then it is more desirable to design light low-cost wings. This can be obtained by, for instance, decreasing the aspect ratio. Companies at early stages in the development, which face a high risk of frequent crashes, should aim to decrease the kite costs by decreasing the kite mass.

The average frequency of tether replacement is of 0.13, meaning that the tether is replaced every about 8 years due to creep. However, its standard deviation is large and it is mainly influenced by the tether material cost p_{te}. A high tether cost drives the optimization towards lower tether stress.

The operational altitude is higher than the hub height of conventional wind turbine with similar rated power. To build a tower is generally beneficial, however the tower height is still below the operational altitude. Its variance depends on parameters related to the tower design (f_{tw} and h_{tw}), the tether material cost p_{te} and the wind shear α. The model used in this work does not penalize design with a short tether, as no dynamic model is included. So, the optimizer aims to reach the high wind speed at high altitudes in the most convenient way, which is a trade-off between tower height and the vertical component of the tether. The elevation angle has small standard deviation.

The kite area has high uncertainty compared to the mean. Its variance depends mainly on the rated power, the electricity price and the wind resources variances. The aspect ratio is low compared to typical glider values, but of the same magnitude of civil aircraft [36]. Its variance is influenced by the variance of parameters related to the structural design (δ_{max}, f_{wing}, p_{wing}), the drag coefficient at zero lift and the frequency of kite replacement. In Figure 15a this dependence is shown. If the kite is replaced often, lower aspect ratios are favourable, to reduce the overall structural mass. For kites with high C_{D0}, higher AR are optimum since higher aspect ratios reduce the induced drag coefficient and therefore help to keep the overall drag low.

The statistics of the take-off climbing angle show that no strategy is generally preferable, from an economic point of view. Indeed, the variables related to the take-off do not show any clear dependence.

The constraint on the rated power is the strongest. The Lagrange multiplier of this limit mainly depends on the Weibull scale parameter and on the electricity price variance. The Lagrange multiplier on the maximum lift coefficient λ_{CL} depends on many parameters, but mainly on $C_{L\,max}$ and C_{D0}. Figure 15b shows this dependence. The constraint on the maximum lift coefficient is strong when C_{D0} is high and $C_{L\,max}$ is low. For high $C_{L\,max}$ it is generally weak. Extremely high lift coefficients are not found to be highly beneficial for the profit. This is in agreement with the finding for the AEP maximization case.

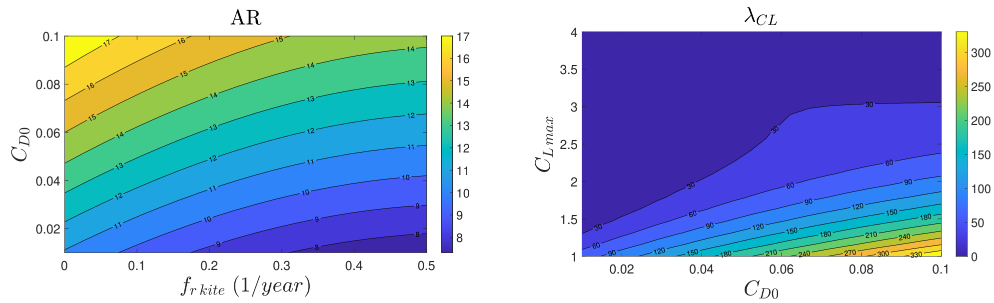

(a) (b)

Figure 15: Meta-model of the aspect ratio as function of the frequency of kite replacement $f_{r\ kite}$ and of the drag coefficient at zero lift C_{D0} (a) and meta-model of the Lagrange multiplier of the maximum lift coefficient as function of the maximum lift coefficient $C_{L\ max}$ and of the drag coefficient at zero lift C_{D0} (b).

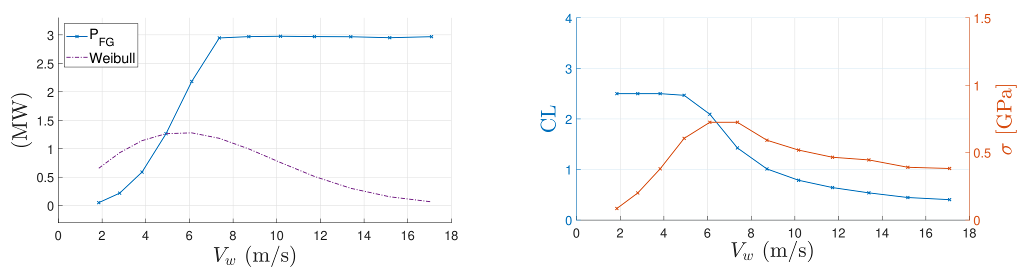

(a) (b)

Figure 16: Power production P_{FG} (a) and lift coefficient and tether stress (b) as function of wind speed for the *Fly-Gen AWES* example.

4.5. Example of a Fly-Gen AWES optimization

The results of a single optimization for a *Fly-Gen AWES* obtained with the mean values of the model parameters uncertainties (Table 3 and 5) are shown, to highlight trends typical of this generation type.

Figure 16a shows the power curve for the *Fly-Gen* example and in Table 7 the main outputs are listed.

In this case, the electronics have a lower share of the costs, compared to the *Ground-Gen* case. The *ICC* is also lower. The optimal span is 62 m with an aspect ratio of 12 lead to a wing area of 322 m^2. The total mass is higher than the solution for *Ground-Gen* case. This is because of the presence of the on-board electronics for a *Fly-Gen* configuration. Looking at the power curve, the rated power is reached at around 7 m/s, leading to a capacity

Table 7: Main outputs of the *Fly-Gen AWES* optimization example.

Output		Units
$LCOE$	30	€/MWh
ICC	1604	k€
OMC	330	k€/year
AEP	17.0	GWh
CF	64.0	%
$C_{structure}$	169	k€
C_{tether}	188	k€
$C_{electronics}$	549	k€
C_{TO}	360	k€
C_{tower}	169	k€
C_{fix}	169	k€
m_{tot}	2439	kg
l_t	445	m
d_t	52	mm
Tower height	125	m
β	17	°
s	62	m
AR	12	-
life$_{te}$	inf	years

factor of 64 %.
In Figure 16b the lift coefficient and the tether stress, as function of the wind speed are shown. The stress reaches the maximum when the rated power is attained. This is in agreement with the power curve description proposed by Vander Lind [26]. In this case, the tether is designed to have a operational life longer than the *AWES* itself.

4.6. Global sensitivity analysis results for Fly-Gen

In Figure A.21 the graphical representation of the total Sobol indices and the outputs statistics of the evaluations are presented.
Fly-Gen AWESs have positive mean profit, meaning that they can be economically attractive and cost competitive. *LCOE* has a mean of 34 €/MWh, higher than the one found for *Ground-Gen*. Its variance mainly depends on the Weibull scale parameter A and of the frequency of kite replacement $f_{r\ kite}$. In Figure 17a the meta-model of this dependence is shown. In regions with high wind resources the cost of energy is low. However, for high value of A,

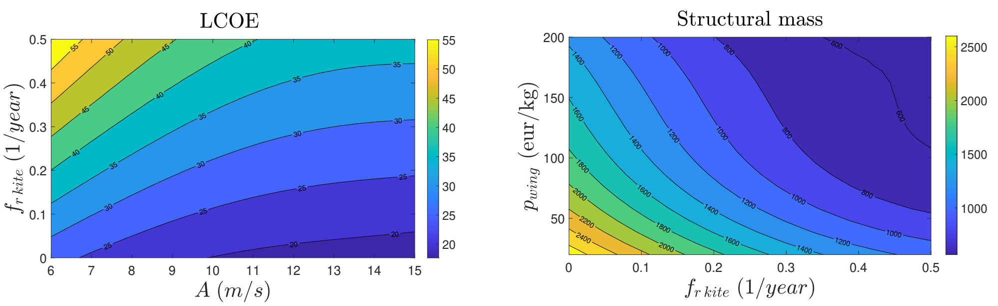

(a) (b)

Figure 17: Meta-model of the LCOE as function of the Weibull scale parameter A and of the frequency of kite replacement $f_{r\ kite}$ (a) and meta-model of the kite structural mass as function of the structural material price p_{wing} and of the frequency of kite replacement $f_{r\ kite}$ (b).

the isolines tend to be horizontal, meaning that the $LCOE$ becomes insensitive the wind conditions at a certain level. The frequency of kite replacement strongly influences the $LCOE$: even if the kite and the on-board electronics needs to be replaced every two years, the system can be designed in a way to have a $LCOE$ similar to conventional wind turbines.

The Initial Capital Cost ICC is lower than for *Ground-Gen*, while the Operation and Maintenance Costs OMC are higher. This is due to the different effect of the frequency of kite replacement $f_{r\ kite}$ on the yearly costs. For every *Fly-Gen* crash, the kite and the on-board electronics need to be replaced and therefore OMC variance is strongly influenced by $f_{r\ kite}$ variance. For every *Ground-Gen* crash, only the kite needs to be replaced: indeed no strong dependence between OMC variance and $f_{r\ kite}$ variance is found (Figure A.20).

By analyzing the average cost breakdown of the initial capital costs of *Fly-Gen*, it turns out that the electronics is still the most expensive part (36%), followed by tether (23 %), take-off structure (16 %) and fix costs (13 %). Also in this case, the structural cost takes a low share in the overall ICC (8 %). This allows the construction of large kites cheaply for a given generator size to attain high capacity factors.

The total mass on average is about 50 % higher than the total mass of a *Ground-Gen*. This is mainly because of the presence of the on-board power electronics. Figure 17b shows how the structural mass varies with the price per kg of the structural material p_{wing} and the frequency of kite replacement

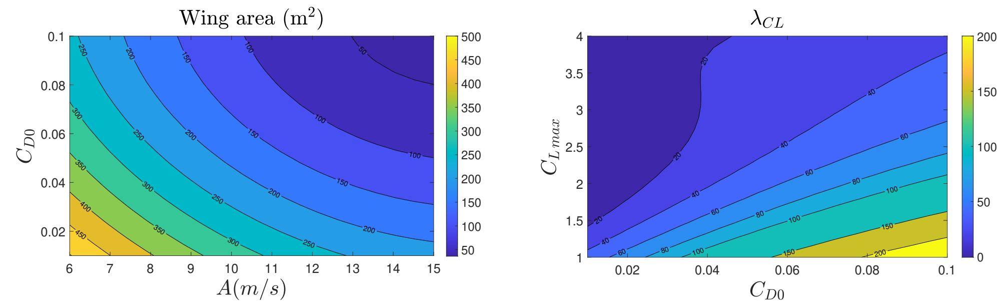

(a) (b)

Figure 18: Meta-model of the kite wing area as function of the Weibull scale parameter A and the drag coefficient at zero lift C_{D0} (a) and meta-model of the Lagrange multiplier on the maximum lift coefficient as function of maximum lift coefficient $C_{L\,max}$ and the drag coefficient at zero lift C_{D0} (b).

$f_{r\,kite}$. The optimal structural mass varies with a factor of approximately four. This shows that there is a lot of uncertainty in the optimal design of *Fly-Gen AWESs*.

The tether is designed to infinite life. The operational altitude, the tether length, the tower height, and the elevation are similar to the *Ground-Gen* case.

The aspect ratio is similar to civil aircraft values [36]. Figure 18a shows how the wing area is influenced by the drag coefficient and by the Weibull scale parameter. The dependence on the wind resources highlights that different wing sizes are optimal for different locations. The dependence on the the drag coefficient at zero lift shows that larger wing area are optimum for kites with large C_{D0}. It has been shown for *Ground-Gen* (Figure 15a) that kites with high C_{D0} requires high AR. This is to reduce the induced drag and keep high system glide ratios. Similar conclusions can be taken for *Fly-Gen*: high C_{D0} implies high aspect ratio, which implies lower wing area because of the structural constraints. *Fly-Gen AWESs* kite designs, at the current early stage of the development, likely have high C_{D0}, due to the structures holding the on-board wind turbines. Thus, low wing areas with higher aspect ratios are expected to be used in the early stages of development. After reducing the drag coefficient by optimizing the aerodynamics, higher wing areas with lower aspect ratio become optimal.

For the AEP maximization, the average of the optimal AR over the parameter space is 30 (Figure 8). The mean aspect ratio for *Ground-Gen* and

Fly-Gen is 12, outlining that a really high aspect ratio is, on average, not attractive from a cost point of view.
The climbing angle α_{TO} shows that a vertical take-off is more convenient. However, the standard deviation is high, meaning that in some cases a linear take-off is preferable. When analysing results related to the take-off, one should consider the simplistic physical and cost model for this sub-system.
The Lagrange multiplier on the rated power is the strongest. Figure 18b shows how λ_{CL} varies with $C_{L\,max}$ and C_{D0}. λ_{CL}, which represents the strength of the upper bound constraint of $C_{L\,max}$, is low at low C_{D0} and at high C_{D0} and high $C_{L\,max}$. If λ_{CL} is low, there is little benefit to increasing $C_{L\,max}$ further. Therefore, extremely high lift coefficients are, on average, not attractive.

4.7. Comparison between Ground-Gen and Fly-Gen AWES

To understand which generation type maximize the profit, the evaluations of the two sensitivity analyses are compared. Figure 19 shows the evaluations for the $LCOE$ as function of the frequency of kite replacement, highlighting the generation type maximizes the objective function. If the kite is not replaced at all, *Fly-Gen* can be more attractive from a cost perspective. If the kite needs to be replaced during the operational life, *Ground-Gen* is preferable. This is related to the cost of the kite that needs to be replaced after a crash.
For low frequency of kite replacement ($f_{r.\,kite} < 0.02\ 1/year$), *Fly-Gen AWESs* can be more convenient mainly because they have a lower initial capital cost, due to the lower electronics cost. Improvements on the cost modelling of the electronic sub-system are necessary, to prove the validity of this trend.

4.8. Global sensitivity analysis results without tower

Since *AWESs* are usually designed to be without tower, global sensitivity analyses for *Ground-Gen* and *Fly-Gen* are run for this case. Figure B.22 and B.23 show the Sobol indices and the statistics for these cases. For both the generation types, the profits decreases slightly. No major changes on the Sobol indices have been found. So, the considerations done in the previous sensitivity analyses are still valid.

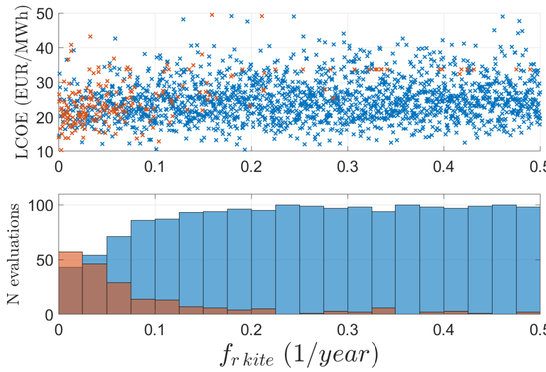

Figure 19: *LCOE* as function of the frequency of kite replacement. In blue the *Ground-Gen* evaluations and in red the *Fly-Gen*.

4.9. Discussion

The *LCOE* of *Ground-Gen* and *Fly-Gen* are similar and low, outlining that both the generation types, with a mature technology, could be disruptive in the energy market. The strength of these technologies is the high capacity factor that can easily be achieved. For a given rated power, the kite structure is, on average, a small portion of the initial capital cost. Thus, large kites can be designed, without a big impact on the total costs. This is the key to reach high capacity factors. High capacity factors imply power generation with low wind conditions. The hours with low wind speeds typically have a high electricity price in regions with a large share of wind energy in the electrical power market. Therefore, power fed into the grid during low wind is extra profitable and more beneficial to the electricity grid.

Comparing the two generation types, *Fly-Gen* can be convenient if the kite control system is reliable. If the kite needs to be replaced often, then *Ground-Gen* is preferable. It should be noted that the results presented in this work are based on an approximate cost model, which is mainly suitable for comparison of the two generation types. The electronics cost for *Fly-Gen* is found to be lower than for *Ground-Gen*, strongly impacting the initial capital cost. This is because the on-board electrical generators spin faster than the generator on the ground. A more detailed cost model of the on-board electronics would be needed to improve the estimates.

For high kite replacement frequency, the optimal kite designs have low structural mass, to reduce the costs after a replacement. For *Ground-Gen*, high aerodynamic performance is not required, from an economic point of view. Therefore, in this case, soft kites could be the good designs for *Ground-Gen*. However, the model used in this work deals exclusively with rigid wing kites, therefore further investigations are necessary.

Investors are attracted to low risk projects. With the assumption that the first commercial *AWESs* will not have a control system fully reliable, investors could be more interested in *Ground-Gen*, to lower the financial exposure of frequent failures.

For *Ground-Gen*, the tether should be designed to have an optimal working life according to the tether cost. For *Fly-Gen*, it is better to have tether designed to infinite life. The tether is found to have a big share in the total cost for both the generation types. Research on how to reduce this cost can have a big impact on *LCOE*. Cheaper tethers will likely be replaced more often. Thus, it could be interesting to further study the creep phenomenon in tethers.

Aspect ratios similar to the ones of commercial aircraft are found to be optimal. This is due to aero-elastic considerations where thicker wings are stiffer. The average structural mass density is of approximately 5 kg/m^2, smaller than typical values for gliders (approximately between 10 and 25 kg/m^2 [31]). This can be explained by the difference in aspect ratio and by the tendency of the optimizer to minimize the structural mass, to reduce costs.

For both the generation types, extremely high maximum lift coefficients are found to have diminishing benefits to the performance. It should be noted that the structural model implemented in this work is typical of rigid wing monoplane configurations. Extremely high lift coefficients are achievable with a multiplane configuration, as this configuration allows for a higher bending stiffness [16] which can cope with higher loadings. If the structural model of multiplanes was implemented, the results concerning the need for an extremely high lift coefficient might change.

This analysis shows that building a tower can be attractive. However, having the ground station placed at the ground (*i.e.* not having the tower) changes only partially the design and the economic performance.

The take-off strategy is not influencing the design. The physical and cost model related to the take-off and landing might be too simplistic to give any interesting or reliable information. The design of this specific sub-system should therefore be carried out with a greater emphasis on safety and reliability considerations compared to operational performance.

In Table 4, the characteristics of a convectional wind turbine of 3.4 MW of

rated power are given (IEA-3.4-130 [32]). For *AWES* designs maximising the profit, the average wing span is 44 m, about one third of the rotor diameter. The *AWES* wing structural masses is approximately 2 % of the three blades total mass. It can be noted that the blade cost is somewhat similar to the wing cost: the considered uncertainties on the wing structural material price are conservative.
The tower cost for wind turbine is equivalent to the tether, tower and take-off sub-system costs. These costs are also somewhat similar, showing that the cost models of these sub-systems are also likely conservative.
Even with these conservative cost models, a *AWES* can be competitive with a conventional wind turbine from a *LCOE* point of view.

5. Conclusions

In this work, the design trends of rigid wing crosswind *AWES* are studied. In a previous paper [13], a unified physical and economical model of *AWESs* which can handle ground and on-board generation is introduced. The unified model is here coupled with system design tools to study optimal designs in detail. In particular, the methods to evaluate the optimal designs are introduced in Section 2. A gradient-based optimization algorithm is used to perform the system design of *AWESs*. The optimization can be considered as a fully deterministic design process that for some model parameters (*i.e.* parameters which are fixed within the optimization problem), performs the system design to maximize *AEP* or the economic profit. A global sensitivity analysis is performed to study how the optimal designs vary for a big variation of the model parameters. This analysis allows to understand which parameters drive the design and how to perform robust designs. This paper used uncertainty quantification based on educated guesses on the input uncertainty primarily to identify important design trends. To develop better estimates on the uncertainties themselves, the technology needs to converge so that a more detailed assessment of the input uncertainties can be obtained.
In Section 3, these methods are used for the evaluation of the physical model, studying designs maximising *AEP*. Given the chosen uncertainties, the key design parameters for the maximization of *AEP* are the maximum lift coefficient and the drag coefficient at zero lift, followed by the wing area. They determine the capacity factor, thus they should be carefully designed. It is found that high aspect ratios are optimal from a purely physical point of view. A method to design strong configurations is proposed: conservative

values can be given to parameters associated with low Sobol indices, and the design performed according to the parameters associated with high Sobol indices.

Finally, it is shown that, as the kite design is not largely influenced by the wind conditions, large area kites could be placed in low wind regions, to obtain high capacity factors.

In Section 4, the same methods are applied to study the configuration designs that maximize the profit. From the design analyzes, it turns out that *Ground-Gen* and *Fly-Gen*, with a mature technology, will be extremely competitive in the energy market. Large area kites can ensure high capacity factors because the kite structure does not represent a large share in the total costs. This is the key to reach a low cost of energy. Aspect ratios similar to commercial aircraft are found to be optimal: this is due to increased airfoil thickness to reduce the overall structural mass and costs. A really high maximum lift coefficient is found unattractive for the AEP maximization and for the profit maximization case: the Lagrange multiplier on the maximum lift coefficient is low in this case. From this analysis, *Fly-Gen* can give slightly higher profit if the kite is rarely or never replaced.

Nomenclature

Acronyms

AEP Annual Energy Production
AWE Airborne Wind Energy
$AWES$ Airborne Wind Energy System
CF Capacity Factor
ICC Initial Capital Cost
$LCOE$ Levelized Cost Of Energy
OC Operation Costs
OMC Operational and Maintenance Costs

Latin Symbols

A Weibull scale parameter
a_{gen} Coefficient for the generator cost.
A_{kite} Wing area
A_{prop} Rotor area of on-board propellers
AR Kite wing aspect ratio
A_{turb} Rotor area of on-board turbines
C_{D0} Kite drag coefficient at zero lift
$C_{electronics}$ Electronics cost

C_{fix} Fix costs
C_L Lift coefficient
$C_{L\,max}$ Upper bound of the lift coefficient design variables (C_L)
$C_\perp$ Drag coefficient of the tether
$C_{structure}$ Structure cost
C_{tether} Tether cost
C_{TO} Take-off sub-system cost
C_{tower} Tower cost
d_t Tether diameter
E_{gen} Power density of the motor/generators.
$f_{el\,FG}$ Factor for the on-board electronic cost
$f_{r\,kite}$ Number of kite replacement in one year
f_{te} Cable manufacturing additional price in case of both structural and electrical components
f_{tw} Coefficient for the manufacturing of the tower
f_{wing} f_{wing} times the spar caps mass models the structural material not included in the wing model
h_{min} Minimum allowed operational altitude
h_{tw} Maximum tower height
i Discount rate
k Weibull form parameter
life_{te} Tether working life
l_t Tether length
m_{tot} Total flying mass mass. Composed by kite mass, on-board additional mass and half of the tether mass
n_y Number of operational years
p_{Ag} Price per unit area of the launch and landing system cost
p_{el} Price of electricity
P_{FG} Power generated by Fly-Gen AWES
P_{GG} Power generated by Ground-Gen AWES
P_{gr} Power ground generated
P_{ob} Power on-board generated
P_r Rated power
p_{te} Price per unit mass of the structural material of the cable.
p_{wing} Price per unit mass of the structural material of the aircraft.
Q_{turb} Percentage of the thrust given by the on-board turbine during the take-off
s Wing span
$SF_{\sigma\,lim}$ Safety factor on the tether strength. The tether strength is 1.5 GPa.
t_A Spar cap thickness close to the tip
t_B Spar cap thickness at half way between tip and tether attachment
t_C Spar cap thickness at the tether attachment and inward

V Line voltage in the tether
V_{in} Cut-in wind speed
V_{out} Cut-out wind speed
V_w Wind speed at a height of 50 m
x_a Spanwise position of the tether attachment

Greek Symbols

α Wind shear coefficient
α_{TO} Climbing angle during the take-off
β Mean elevation angle
Δ Additional kite inclination due to the gravitational force
δ_{max} Percentage of the span: maximum tip and central displacement.
η_d Minimum efficiency due to induction factor of the on-board turbines
η_{in} Efficiency of reel-in phase
η_{out} Efficiency of reel-out phase
η_{pr} Efficiency of the propellers with respect to disc theory
η_t Efficiency of the on-board generation
$\eta_{t\ pr}$ Efficiency of the turbines used in propeller mode with respect to disc theory
γ_{in} Ratio between reel-in velocity and wind velocity
γ_{out} Ratio between reel-out velocity and wind velocity
γ_t Ratio between thrust force given by on-board wind turbines and aerodynamic drag
λ_{CL} Lagrange multiplier on the maximum lift coefficient constraint
λ_{Prated} Lagrange multiplier on the rated power constraint
λ_{te} Lagrange multiplier on the tether strenght constraint
Π Annual profit
ρ_{wing} Structural material density

References

[1] U. Ahrens, M. Diehl, R. Schmehl (Eds.), Airborne Wind Energy, Green Energy and Technology, Springer, 2013. doi:10.1007/978-3-642-39965-7.

[2] R. Schmehl (Ed.), Airborne Wind Energy - Advances in Technology Development and Research, Green Energy and Technology, Springer, Singapore, 2018. doi:10.1007/978-981-10-1947-0.

[3] R. Schmehl, O. Tulloch, Airborne Wind Energy Conference 2019: (AWEC 2019), Glasgow, United Kingdom, 2019. doi:10.4233/uuid:57fd203c-e069-11e9-9fcb-441ea15f7c9c.

[4] M. Loyd, Crossswind Kite Power, Journal of Energy 4 (3) (1980) 106–111.

[5] Kikepower, `https://kitepower.nl/` (2019 (accessed December 16, 2019)).

[6] Enerkite, `https://www.enerkite.de/en/` (2019 (accessed December 16, 2019)).

[7] Ampyx Power, `https://www.ampyxpower.com/` (2019 (accessed December 16, 2019)).

[8] Kitemill, `http://www.kitemill.com/` (2019 (accessed December 16, 2019)).

[9] Makani Power, `https://makanipower.com/` (2019 (accessed December 16, 2019)).

[10] Kitex, `https://kitex.tech/` (2019 (accessed December 16, 2019)).

[11] A. Cherubini, A. Papini, R. Vertechy, M. Fontana, Airborne Wind Energy: A review of the technologies, Renewable and Sustainable Energy Reviews 51 (2015) 1461–1476. `doi:10.1016/j.rser.2015.07.053`.

[12] F. Trevisi, Configuration optimisation of kite-based wind turbines, Master's thesis, Technical University of Denmark (2019). `doi:10.13140/RG.2.2.24256.28160`.

[13] F. Trevisi, M. Gaunaa, M. McWilliam, Unified engineering models for the performance and cost of Ground-Gen and Fly-Gen crosswind Airborne Wind Energy Systems, Renewable Energy 162 (2020) 893–907. `doi:10.1016/j.renene.2020.07.129`.

[14] J. Heilmann, C. Houle, Economics of Pumping Kite Generators, in: U. Ahrens, M. Diehl, R. Schmehl (Eds.), Airborne Wind Energy. Green Energy and Technology. Springer, Singapore, 2013, pp. 271–284. `doi:10.1007/978-3-642-39965-7\_15`.

[15] C. Grete, Optimization, Scaling and Economics of Pumping Kite Power Systems, MSc thesis, Delft University of Technology (2014).

[16] F. Bauer, R. M. Kennel, C. M. Hackl, F. Campagnolo, M. Patt, R. Schmehl, Drag power kite with very high lift coefficient, Renewable Energy 118 (2018) 290–305. doi:10.1016/j.renene.2017.10.073.

[17] fmincon, https://se.mathworks.com/help/optim/ug/fmincon.html (2019 (accessed July 7, 2019)).

[18] J. Nocedal, S. Wright, Numerical optimization, series in operations research and financial engineering, 2006.

[19] S. Marelli, B. Sudret, UQLAB: a framework for Uncertainty Quantification in MATLAB, The 2nd International Conference on Vulnerability and Risk Analysis and Management (ICVRAM 2014) (2014) 2554–2563.

[20] S. Raychaudhuri, Introduction to monte carlo simulation, Winter Simulation Conference (2008) 91–100doi:10.1109/WSC.2008.4736059.

[21] B. Sudret, S. Marelli, J. Wiart, Surrogate models for uncertainty quantification: An overview, 2017 11th Eur. Conf. Antennas Propagation, EUCAP 2017 (2017) 793–797doi:10.23919/EuCAP.2017.7928679.

[22] I. M. Sobol, Sensitivity analysis for nonlinear mathematical models, Mathematical Modeling & Computational Experiment (1993) 407–414.

[23] G. Licitra, J. Koenemann, A. Bürger, P. Williams, R. Ruiterkamp, M. Diehl, Performance assessment of a rigid wing Airborne Wind Energy pumping system, Energy 173 (2019) 569–585. doi:10.1016/j.energy.2019.02.064.

[24] G. Licitra, S. Sieberling, S. Engelen, P. Williams, R. Ruiterkamp, M. Diehl, Optimal control for minimizing power consumption during holding patterns for airborne wind energy pumping system, 2016 European Control Conference (ECC) (2016) 1574–1579 doi:10.1109/ECC.2016.7810515.

[25] R. Ruiterkamp, S. Sieberling, Description and Preliminary Test Results of a Six Degrees of Freedom Rigid Wing Pumping System, in: U. Ahrens, M. Diehl, R. Schmehl (Eds.), Airborne Wind Energy, 2013, pp. 443–458. doi:10.1007/978-3-642-39965-7_26.

[26] D. Vander Lind, Analysis and Flight Test Validation of High Performance Airborne Wind Turbines, in: U. Ahrens, M. Diehl, R. Schmehl (Eds.), Airborne Wind Energy, 2013, pp. 473–490. doi:10.1007/978-3-642-39965-7_28.

[27] Makani Power, INC., Response to the Federal Aviation Authority, Docket No.: FAA-2011-1279; Notice No. 11-07; Notification for Airborne Wind Energy Systems (AWES).

[28] A. Cherubini, Fundamentals of Airborne Wind Energy a course for engineering students and researchers, Universidad Carlos III de Madrid (2017).

[29] L. Fagiano, S. Schnez, On the take-off of Airborne Wind Energy Systems based on rigid wings., Renewable Energy 107 (2017) 473–488. doi:10.1016/j.renene.2017.02.023.

[30] Magnax, https://www.magnax.com/technology (2019 (accessed April 19, 2019)).

[31] Glider review, http://www.gliderreview.com/ (2019 (accessed May 11, 2019)).

[32] P. Bortolotti, H. C. Tarrés, K. Dykes, K. Merz, L. Sethuraman, D. Verelst, F. Zahle, IEA Wind TCP Task 37: Systems Engineering in Wind Energy-WP2.1 Reference Wind Turbines (2019). doi:10.2172/1529216.

[33] Grant Thornton, Renewable energy discount rate survey results – 2017.

[34] K. Capion, M. Stryg, R. K. Poulsen, Electricity Price Outlook 2018. Perspectives for the power price in North West Europe towards 2035 (2018), Dansk Energi.

[35] R. Bosman, V. Reid, M. Vlasblom, P. Smeets, Airborne Wind Energy Tethers with High-Modulus Polyethylene Fibers, in: U. Ahrens, M. Diehl, R. Schmehl (Eds.), Airborne Wind Energy. Green Energy and Technology. Springer, Singapore, 2013, pp. 563–585. doi:10.1007/978-3-642-39965-7_33.

[36] L. Jenkinson, P. Simpkin, D. Rhodes, Civil jet aircraft design, Arnold, 1999.

Appendix A. Global sensitivity analysis results

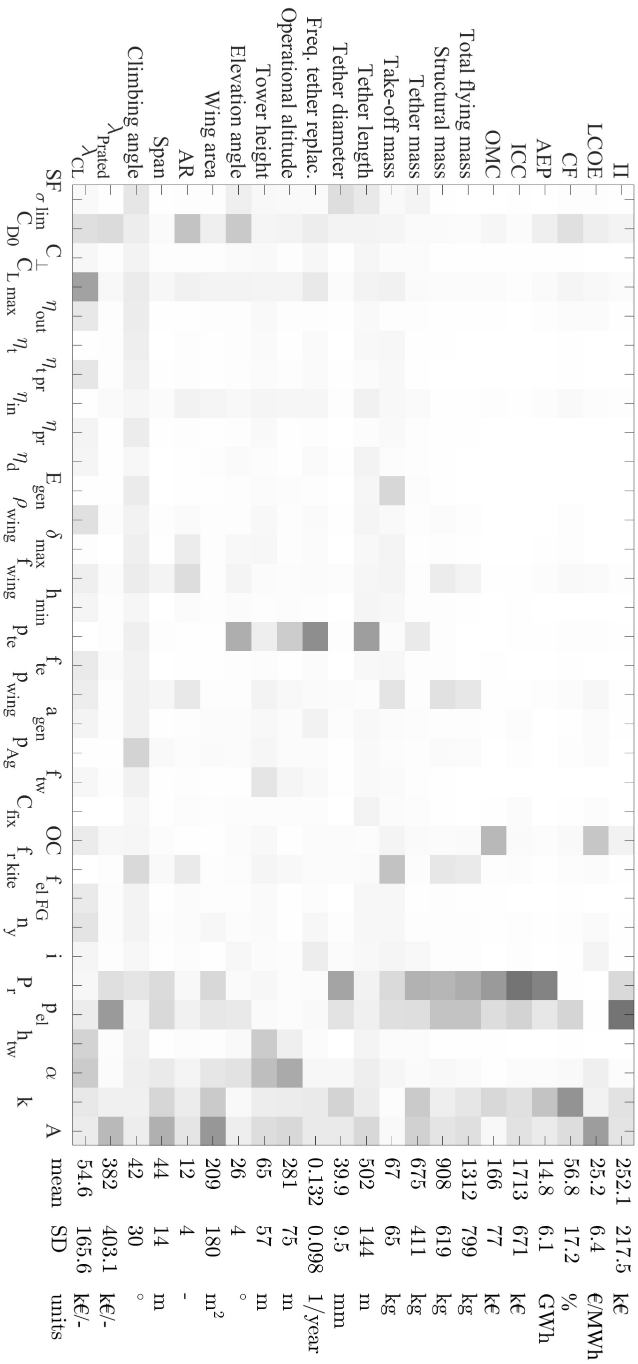

Figure A.20: Graphical visualization of the total Sobol indices and output statistics for the profit maximization for a *Ground-Gen AWES*.

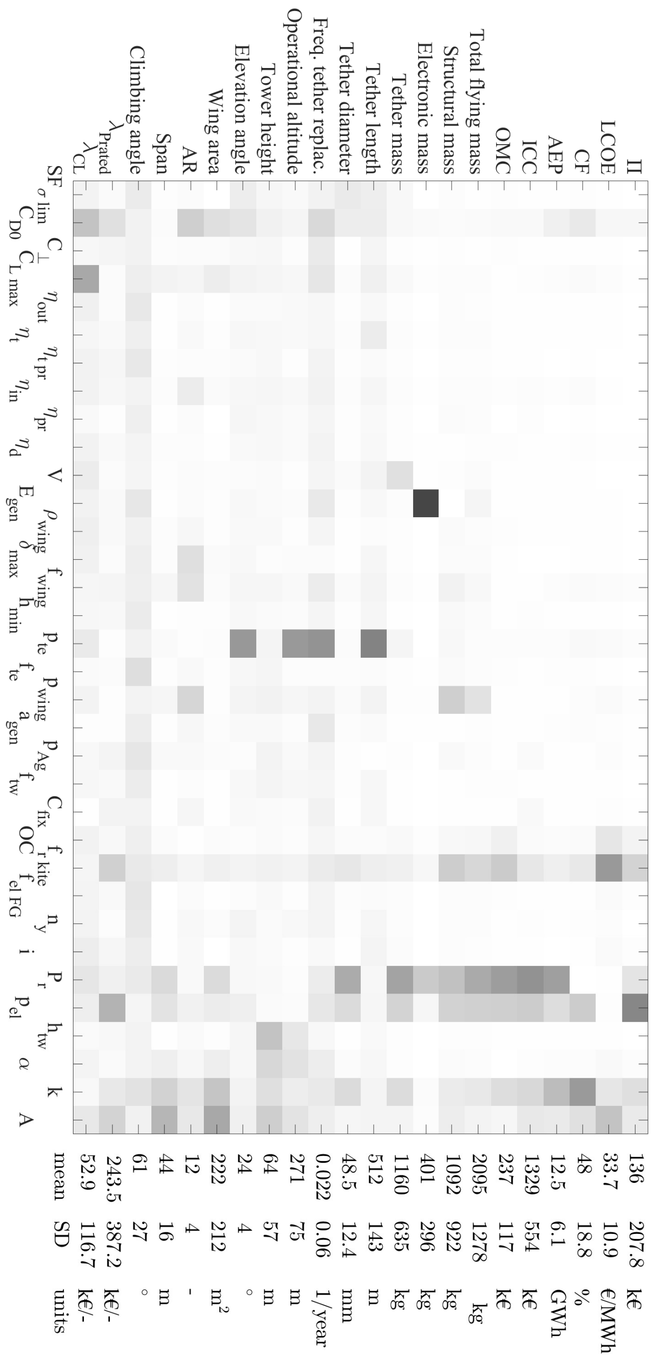

Figure A.21: Graphical visualization of the total Sobol indices and output statistics for the profit maximization for a *Fly-Gen AWES*.

Appendix B. Global sensitivity analysis results without tower

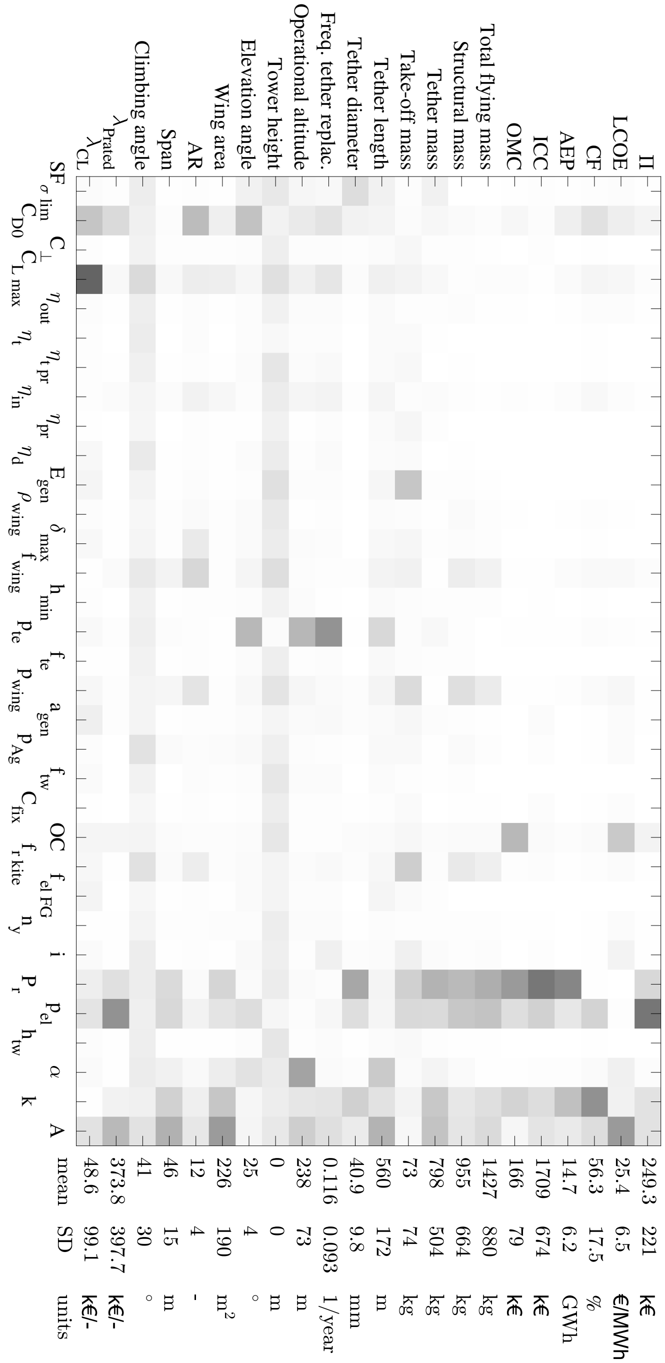

Figure B.22: Graphical visualization of the total Sobol indices and output statistics for the profit maximization for a *Ground-Gen AWES* and no tower.

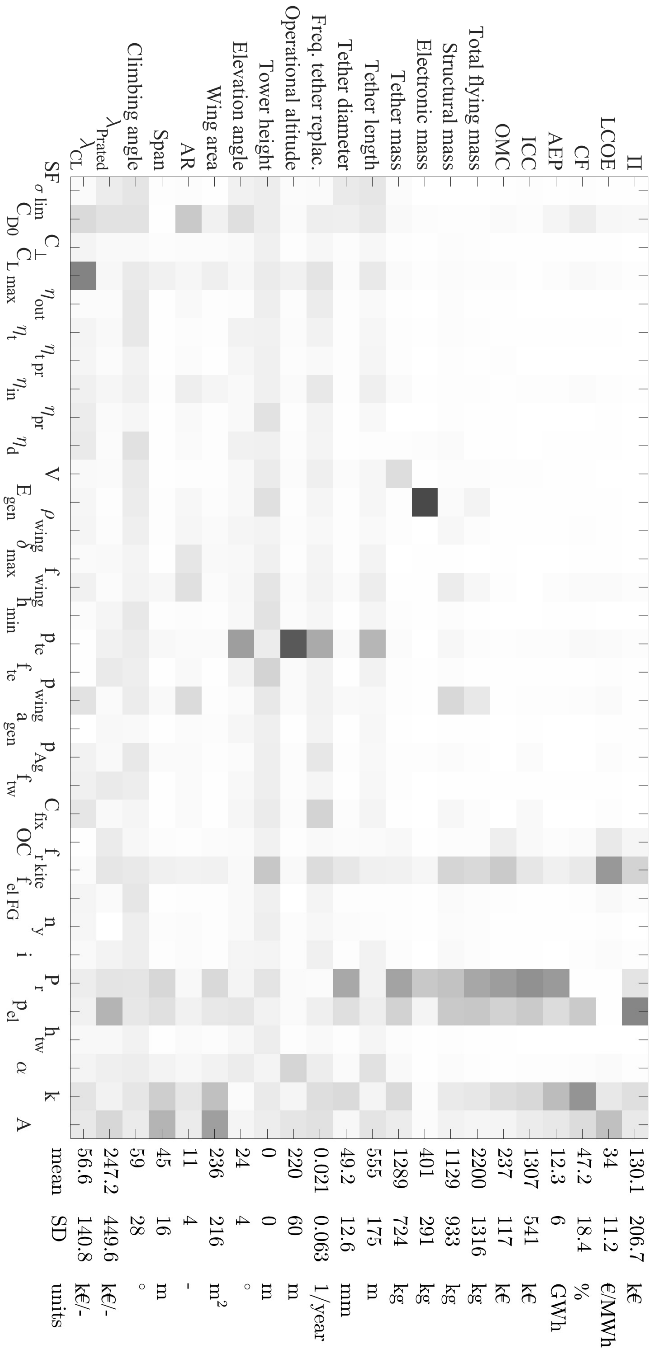

Figure B.23: Graphical visualization of the total Sobol indices and output statistics for the profit maximization for a *Fly-Gen AWES* and no tower.